Journal of Alloys and Compounds 970 (2024) 172633

Contents lists available at ScienceDirect

Journal of Alloys and Compounds

journal homepage: www.elsevier.com/locate/jalcom

Design and development of porous CoCrFeNiMn high entropy alloy (Cantor alloy) with outstanding electrochemical properties

Talha Abid [a], M. Aftab Akram [a], Talha Bin Yaqub [b], M. Ramzan Abdul Karim [c], Filipe Fernandes [b,d], Muhammad Farooq Zafar [e], Khurram Yaqoob [a,*]

[a] School of Chemical and Materials Engineering (SCME), National University of Sciences and Technology (NUST), H-12 Islamabad, Pakistan
[b] University of Coimbra, CEMMPRE - Centre for Mechanical Engineering Materials and Processes, Department of Mechanical Engineering, Rua Luís Reis Santos, 3030–788 Coimbra, Portugal
[c] Department of Materials Science and Engineering, Ghulam Ishaq Khan Institute of Engineering Sciences and Technology, Topi, Swabi 23640, KPK, Pakistan
[d] ISEP School of Engineering, Polytechnic of Porto, Rua Dr. António Bernardino de Almeida 431, 4200072 Porto, Portugal
[e] Centre of Excellence in Science & Applied Technologies, Islamabad, Pakistan

ARTICLE INFO

Keywords:
High entropy alloys
Porous alloys
Foams
Cantor alloy
Electrochemical properties

ABSTRACT

CoCrFeNiMn high entropy alloys are among the most well-studied high entropy alloys that exhibit reasonable strength and outstanding ductility. In the present study, porous CoCrFeNiMn foams have been developed by the addition of copper in the base high entropy alloy by arc melting followed by its removal through an electrochemical dealloying process. Microstructure characterization of the as-cast samples confirmed limited solubility of copper in the matrix while the majority of the copper was found to segregate to interdendritic areas. Removal of copper from the interdendritic areas was successfully carried out by an electrochemical dealloying process which resulted in the development of foams with interconnected porosity. CoCrFeNiMn foams with different levels of porosities were successfully developed by varying the amount of added copper in the base HEA and its removal by a dealloying process. The electrochemical performance of the developed foams was assessed by cyclic voltammetry (CV), galvanostatic charge-discharge (GCD), and electrochemical impedance spectroscopy (EIS). One of the developed foams was found to exhibit an areal capacitance of 1.56 F cm^{-2} at 2 mA cm^{-2} which is more than 2x times higher than the value reported for recently developed porous AlCoCrFeNi high entropy foam. Developed foam, besides showing excellent values of areal capacitance, demonstrated capacitance retention of 114.6% after 5000 cycles at 8 mA cm^{-2}. The excellent electrochemical performance of the developed high entropy foams exhibits their potential to be used as electrode materials for supercapacitor applications and was attributed to the insertion of interconnected porosity in the base HEA.

1. Introduction

Significant efforts have been made to develop materials with outstanding electrochemical performances in response to the increasing demand for materials for energy storage applications [1–15]. Supercapacitors have gained remarkable attention in this regard owing to their high-power density, fast charging/discharging rates, and long cyclic life. Carbon materials, conducting polymers, transition metal/ metal oxides, metal hydroxides, and nanocomposite materials have been studied as materials for supercapacitor electrodes [16–29]. Among the aforementioned materials, metal/metal oxides have been extensively explored as supercapacitor electrodes mainly because of their fast surface redox reactions and larger energy densities than EDLCs. The development of electrode materials with excellent electrochemical performance is still an outstanding issue despite the advancements in supercapacitor technology.

High entropy alloys (HEAs) are a relatively new class of metal alloys, which, unlike the conventional alloys, are composed of five or more principal elements in equal proportions [30]. HEAs have shown an outstanding combination of mechanical properties as well as magnetic properties and are being considered as an alternative to conventional materials for demanding structural applications [31–44]. The potential of high entropy alloys for energy storage and catalysis applications has been explored in some of the recent studies [45–48]. As the charge

* Corresponding author.
E-mail address: khurram.yaqoob@scme.nust.edu.pk (K. Yaqoob).

https://doi.org/10.1016/j.jallcom.2023.172633
Received 12 June 2023; Received in revised form 19 October 2023; Accepted 22 October 2023
Available online 24 October 2023
0925-8388/© 2023 Elsevier B.V. All rights reserved.

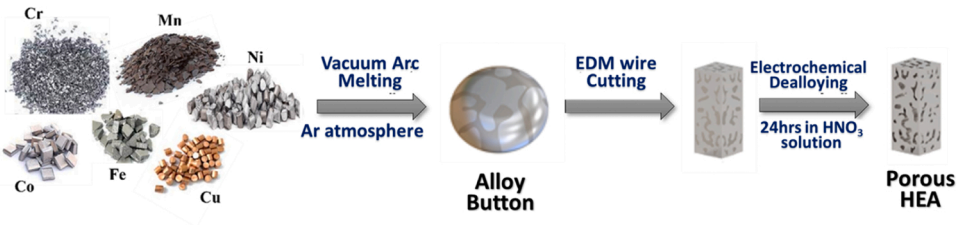

Fig. 1. Schematic illustration of experimental procedure.

Table 1
Enthalpy of mixing (ΔH_{mix}) for the atomic pairs of selected HEA system [62].

	Co	Cr	Fe	Ni	Mn	Cu
Co	0	-4	-1	0	+ 5	+ 6
Cr	-	0	-1	-7	+ 2	+ 1
Fe	-	-	0	-2	0	+ 1
Ni	-	-	-	0	-8	+ 4
Mn	-	-	-	-	0	+ 4
Cu	-	-	-	-	-	0

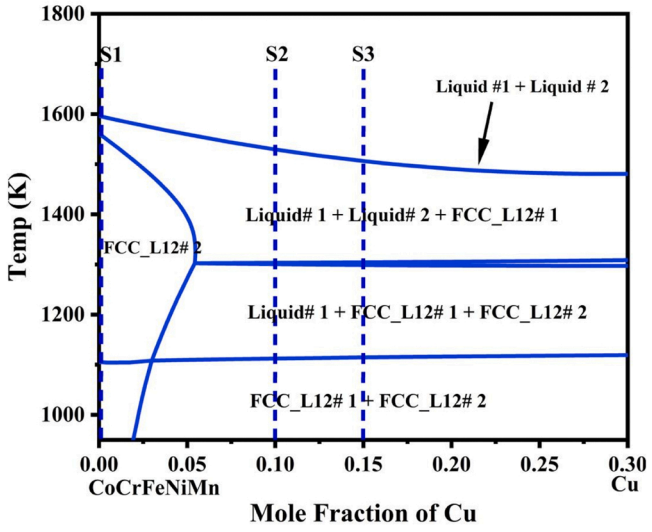

Fig. 2. Pseudo binary phase diagram of CoCrFeNiMn-Cu.

storage capability of the electrode materials depends on the specific surface area and electrical conductivity of the electrode material [25], the capacitive performance of HEAs could be significantly improved by the insertion of porosity [49–51] in high electrical conductivity high entropy alloys. The present study is focused on the development of porous HEA and exploring their potential for energy storage applications.

A variety of synthesis routes have been reported for the development of porous electrodes with high surface area [52–55]. The carbothermal shock (CTS) method is used to develop multicomponent HEA nanoparticles (NPs). This method allows the fabrication of a range of multicomponent NPs with varying compositions and pore sizes by precisely controlling the CTS parameters. However, the productivity of the HEA NPs through the CTS method is low. Sol-gel technique has been used for the fabrication of composite materials with mesoporous assembly and high surface area. The post-heating temperature significantly affects the pore sizes which influences the performance of the electrode material. Selective phase dissolution is a facile synthesis technique applied for preparing nano porous metals or alloys by selectively removing the less stable components and retaining more stable phases or components. The formation of the nano-porous structure increases the surface area and facilitates the diffusion of the electrolyte ions inside the porous channels, thus enhancing the electrochemical performance of the electrode.

Few attempts have been made to evaluate the electrochemical performance of porous HEA systems. AlCoCrFeNi nano porous HEA was fabricated by the selective phase dissolution of HEA precursors [45]. The fabricated nano porous HEA electrode exhibited areal capacitance of 0.7 F cm^{-2} and demonstrated excellent cyclic stability, retaining ~97% of the initial capacitance. (FeCoCrMnNi)C porous high entropy carbide (HEC) was synthesized using the sol-gel synthesis route with a sintering temperature under 1500ºC [52]. The prepared HEC demonstrated a specific capacity of 169.7 F g^{-1} at a current density of 0.5 A g^{-1} and retained 81% of the initial capacity after 10,000 cycles. The developed electrode material also exhibited an energy density of 15.08 Wh kg^{-1} which has been reported to be greatly improved compared to other high entropy materials. $FeCrCoMnNiAl_{0.75}$ HEA has been fabricated through high-frequency induction melting followed by the selective phase dissolution to obtain high entropy metallic frameworks (HEMFs). The formation of metallic frameworks (MFs) because of selective phase dissolution of the cubic fcc phases increased the surface area of the HEMFs. The HEMFs were decorated with MnO_2 layers for pseudocapacitor functionalization. The developed MnO_2/MFs composite with a large effective surface area showed a specific capacitance of 961 F g^{-1} at 5 A g^{-1} current density [56]. High entropy pyrochlore oxide (LaY) $(Zr_{0.5}Ti_{0.5}Ce_{0.5}Hf_{0.5})O_7$ (HEPO) was developed using the sol-gel method combined with low-temperature sintering technology in order to explore its electrochemical potential for energy storage [57]. The fabricated materials exhibited the specific capacitance of 703.3 F g^{-1} in 1 M Na_2SO_4 electrolyte. In addition, the electrode demonstrated excellent cyclic stability by retaining 97.9% of the initial capacitance after 10,000 cycles.

CoCrFeNiMn is one of the most popular and most well-studied high entropy alloy that showed excellent ductility, excellent fracture toughness, and good corrosion resistance. In the present study, we aim to insert interconnected porosity in CoCrFeNiMn alloy to increase its surface area and evaluate the effect of insertion of porosity on its electrochemical performance. A novel strategy has been adopted which is based on the insertion of a partially soluble filler metal to the base HEA by arc melting followed by its removal with the help of an electrochemical dealloying process for the development of interconnected porosity. Foams with different porosity levels have been developed by varying the amount of filler metal and the effect of insertion of porosity on microstructure, crystal structure, and electrochemical performance has been studied.

2. Experimental techniques

Cobalt (99.95% pure), chromium (99.95% pure), iron (99.95% pure), nickel (99.95% pure), manganese (99.95% pure) and copper (99.95% pure), in the form of elemental pellets, were used as raw materials for the development of high entropy alloys. Constituents of envisaged high entropy alloys were placed in a hemispherical water-cooled copper mold and the chamber of the furnace was initially evacuated to 3×10^{-5} mbar. High-purity argon gas was then injected into the furnace chamber for the melting of high entropy alloys under a controlled atmosphere. The titanium getter was melted, before the

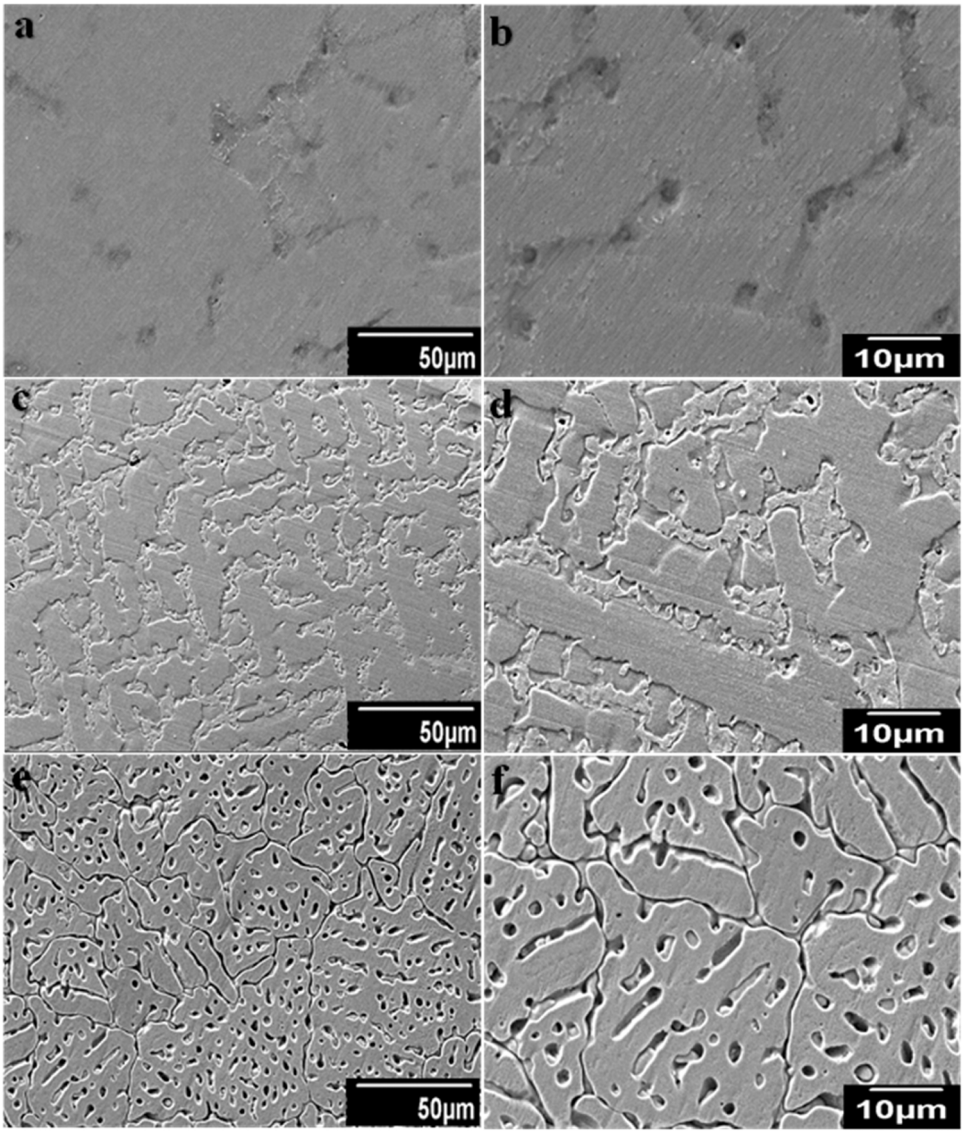

Fig. 3. SEM images of **(a,b)** as-cast S1, **(c,d)** as-cast S2 and **(e,f)** as-cast S3.

melting of the desired HEA, to dissolve any traces of oxygen remaining in the chamber. Each sample was melted for around 30 s, flipped over after each melting, and melted again. This process was repeated five times to ensure chemical homogeneity. Samples for microstructure, crystal structure, and electrochemical characterization were taken out from the alloy button with the help of an electrical discharge machine (EDM) wire cutting. Microstructural characterization and elemental analysis of the developed samples were carried out with the help of a scanning electron microscope (JEOL-JSM-6490LA) equipped with energy dispersive X-ray spectroscopy (EDS) detector. Crystal structure characterization of developed samples was carried out by performing X-ray diffraction measurements on a Bruker D2 Phaser (equipped with Cu K_α radiation) in the 2θ° scan range of 20° - 90°. An electrochemical dealloying process was used to remove copper from interdendritic areas of as-cast high entropy alloys for the development of corresponding high entropy foams. Samples were immersed in the 5% aqueous solution of nitric acid (70%) for 24 h for electrochemical dealloying. A schematic illustration of the foam-making process is shown in Fig. 1.

Electrochemical characterization of the developed as-cast high entropy alloys and their respective foams was conducted in a three-electrode cell configuration by using a potentiostat (Interface 1010E, Gamry Instruments, USA). Cyclic voltammetry and galvanostatic charge-discharge tests were carried out in 2 M KOH aqueous electrolyte with HEA electrode, platinum (Pt) wire, and Hg/HgO serving as working electrode, counter electrode, and reference electrode respectively. The exposed surface area of HEA working electrodes for all electrochemical measurements was around 3×3 mm. Areal capacitance from the GCD curves was calculated by using Equation 1.

$$AC = \frac{I}{S} X \frac{t}{\Delta V} \tag{1}$$

Where I is the current (mA), t is the discharging time (sec), S is the exposed geometric area, and ΔV is the discharging voltage (V). Electrochemical impedance spectroscopy (EIS) was carried out in the frequency range of 100 KHz-10mHz with 10 mV potential amplitude.

3. Results and discussion

CoCrFeNiMn is a well-studied composition that exhibits single-phase fcc microstructure [58–60]. The method proposed for the development of porous CoCrFeNiMn HEA is an adoption of the method used for the development of CoCrFeNi foams and is based on the addition of such a filler metal to base HEA system that tends to segregate at the interdendritic regions during solidification [61]. Subsequent removal of the filler

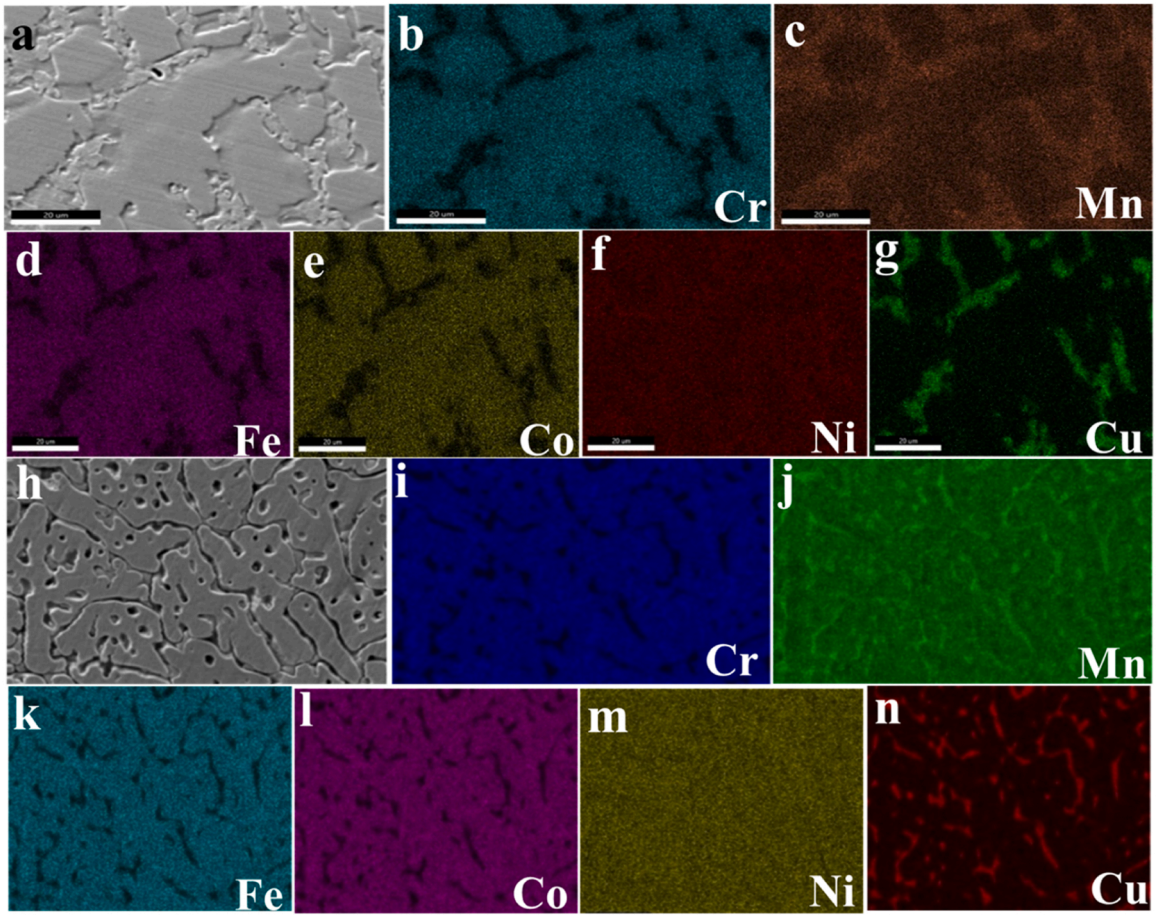

Fig. 4. EDS mapping of **(a-g)** as-cast S2 & **(h-n)** as-cast S3 HEA.

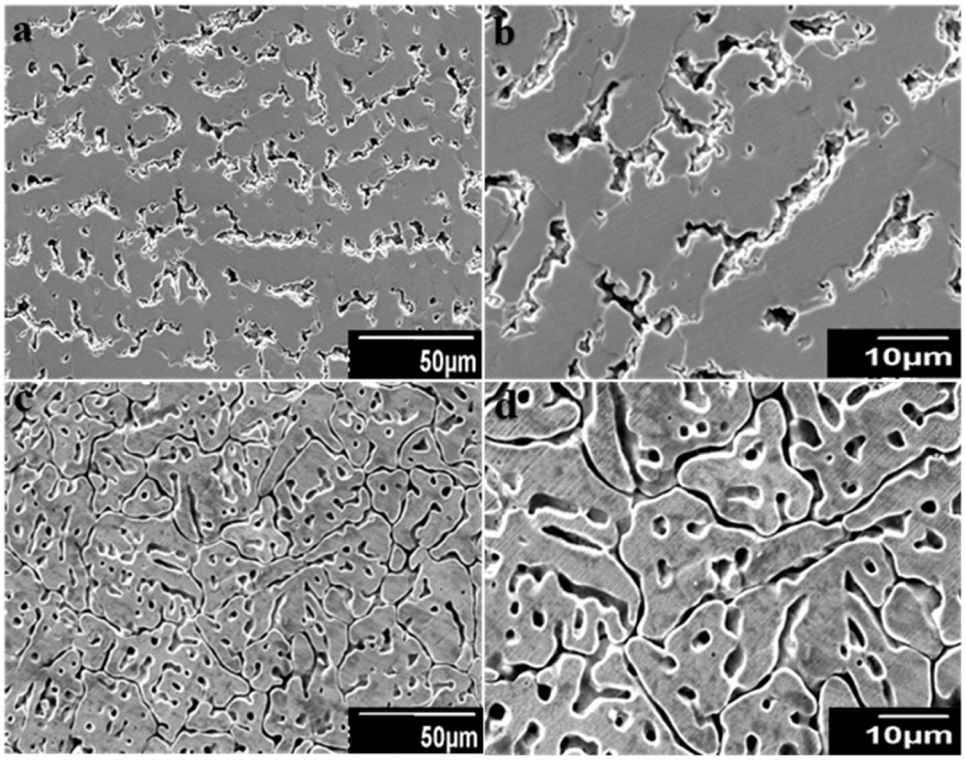

Fig. 5. SEM micrographs of **(a,b)** FS2 and **(c,d)** FS3.

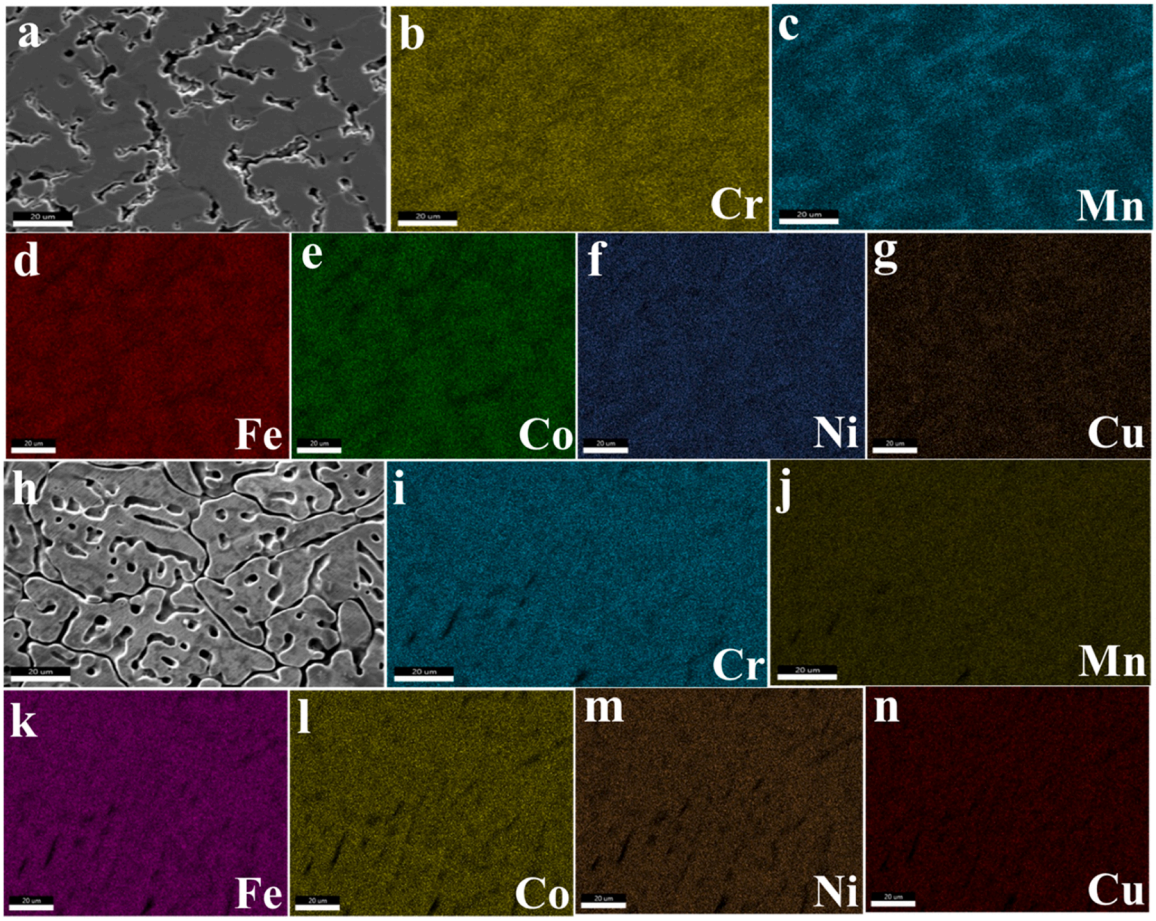

Fig. 6. EDS mapping of **(a-g)** FS2 & **(h-n)** FS3 HEA.

metal from interdendritic areas can help in the development of 3D interconnected porosity. Copper possesses positive enthalpy of mixing with all components of the selected HEA, it is therefore believed that it will tend to segregate to interdendritic areas during solidification. Subsequent removal of copper from interdendritic areas would help in the development of interconnected porosity. Enthalpy of mixing of the constituent elements of the selected HEA system with copper is given in Table 1.

To verify aforementioned hypothesis, pseudobinary phase diagram of CoCrFeNiMn-Cu HEA (shown in Fig. 2) was calculated with the help of Thermocalc software using TCHEA database. The maximum solubility of copper in CoCrFeNiMn HEA, as shown in Fig. 2, is around 6% at 1300 K. Any addition of Cu beyond its maximum solubility in CoCrFeNiMn HEA would lead to its segregation to the interdendritic areas. CoCrFeNiMn high entropy alloy compositions with varying amounts of copper (0 at%, 10 at%, 15 at%) were shortlisted for the present study and were named as S1, S2, and S3 respectively. Shortlisted compositions are also shown as dotted lines on the calculated pseudo-binary phase diagram shown in Fig. 2.

3.1. Microstructural analysis

Microstructural investigation of the as-cast high entropy alloys and their respective foams obtained after electrochemical dealloying was carried out with the help of scanning electron microscope. SEM images of the S1, S2, and S3 are shown in Fig. 3. The S1 sample, as shown in Fig. 3(a,b), showed the presence of only light grey areas corresponding to the HEA matrix. SEM images of S2 and S3 samples showed the presence of HEA matrix and interdendritic areas. The amount of the interdendritic areas was found to increase with the increase in the amount of added copper. EDS mapping was carried out to investigate elemental distribution in the studied samples. EDS maps of the S2 and S3 samples are shown in Fig. 4. As shown in Fig. 4, Co, Cr, and Fe, were found to be uniformly distributed throughout the matrix. Nickel was found to be uniformly distributed in both the matrix and interdendritic areas while copper and manganese were found to be relatively more concentrated in the interdendritic areas (Fig. 4(g) and Fig. 4(n)). Electrochemical dealloying of S2 and S3 samples was carried out by immersing them in 5% aqueous solution of nitric acid (70%) solution for 24 h. SEM, EDS, and XRD analysis was carried out to evaluate the effect of dealloying on the microstructure and crystal structure of the studied samples. Foams of the S2 and S3 samples obtained after the dealloying process were named as FS2 and FS3 respectively. SEM images of FS2 and FS3 samples are shown in Fig. 5. As shown in the Fig. 5, copper was successfully removed from the interdendritic areas for the development of interconnected porosity (1.5–3 μm). Elemental distribution in the dealloyed samples was studied with the help of EDS mapping. EDS maps of the FS2 and FS3 samples, shown in Fig. 6, confirmed removal of copper from interdendritic areas.

3.2. Phase analysis

Crystal structure characterization of the as-cast and dealloyed samples was carried out with the help of XRD measurements. XRD patterns of as-cast samples, as shown in Fig. 7(a), clearly showed presence of two FCC phases. By combining the SEM and XRD results, it was concluded that FCC-1 corresponded to the matrix phase and FCC-2 corresponded to the interdendritic areas. Relative intensity of the peaks corresponding to the FCC-2 phase was comparatively higher in S3 than in S2. The higher relative intensity of the FCC-2 in the sample S3 was attributed to a

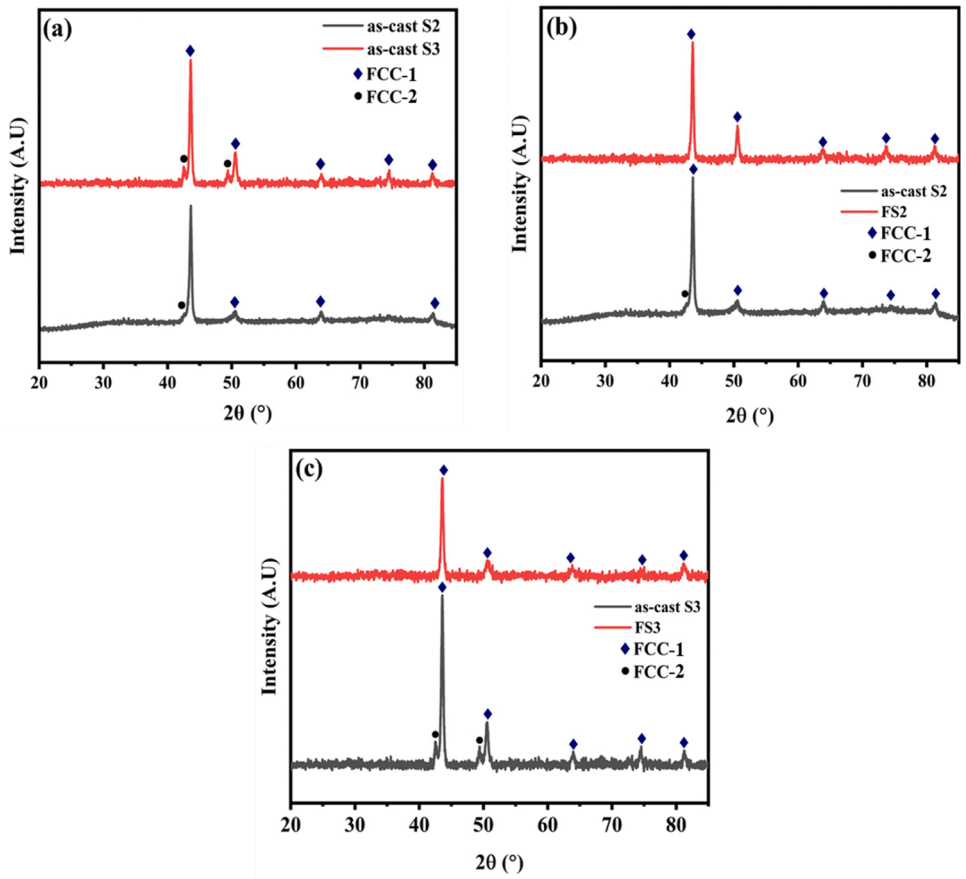

Fig. 7. XRD patterns of **(a)** as-cast S2& S3 sample **(b)** as-cast S2 and FS2 and **(c)** as-cast S3 and FS3.

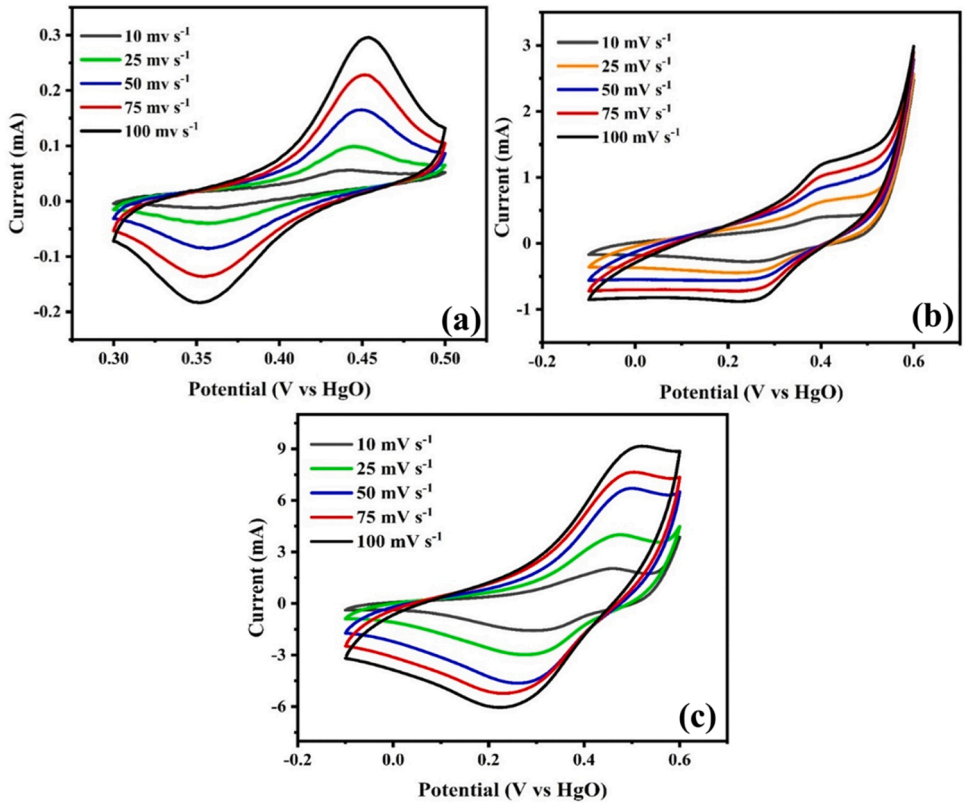

Fig. 8. Cyclic voltammetry curves for **(a)** as-cast S1, **(b)** FS2 and **(c)** FS3 at various scan rates.

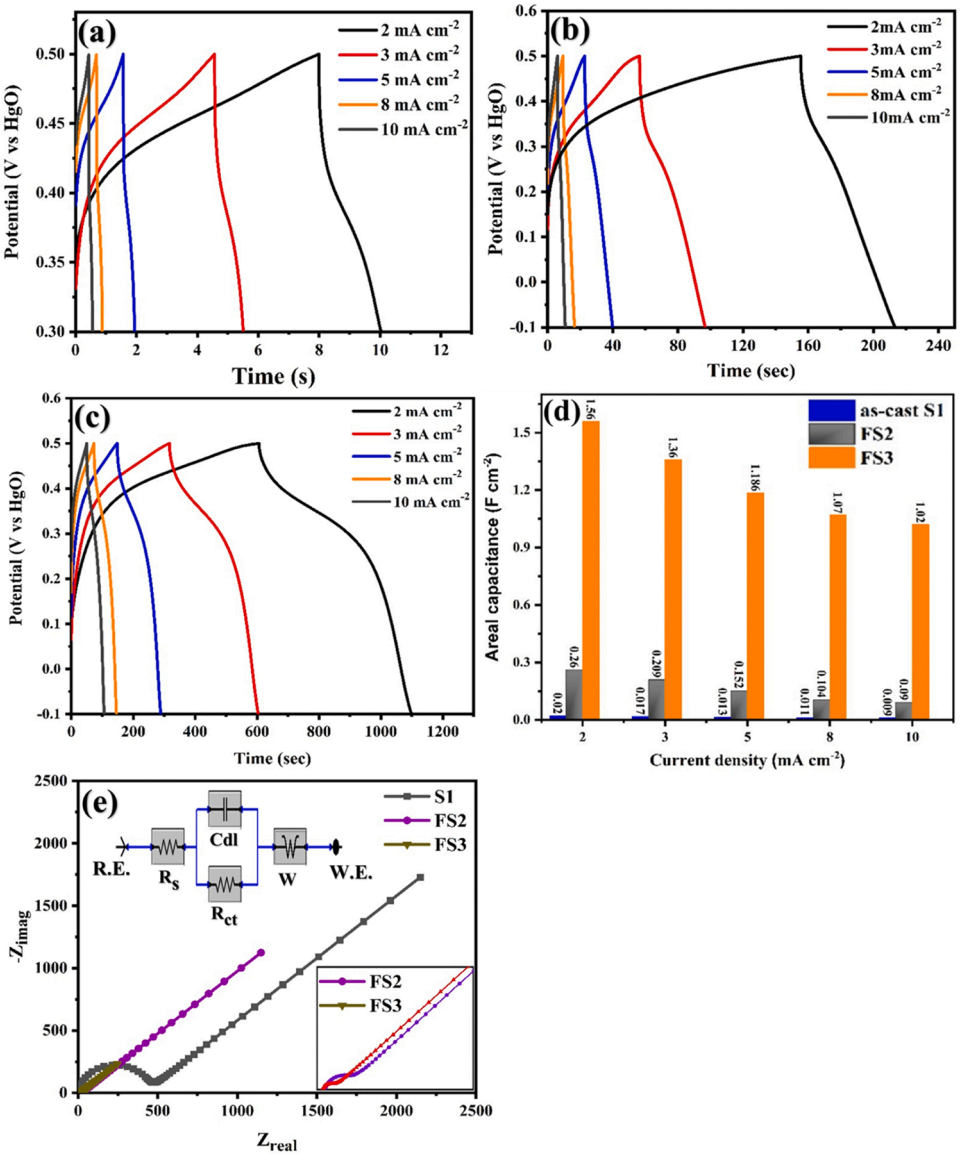

Fig. 9. Charge/discharge curves of **(a)** S1, **(b)** FS2, **(c)** FS3 at various scan rates **(d)** comparison of areal capacitance of HEA electrodes and **(e)** Nyquist plots of S1, FS2 and FS3.

Table 2
Areal capacitance values of S1, FS2, and FS3 at different current densities (calculated from GCD curves).

Current Density (mA cm^{-2})	Areal Capacitance (F cm^{-2})		
	S1	FS2	FS3
2	0.02	0.26	1.56
3	0.017	0.209	1.36
5	0.013	0.152	1.186
8	0.011	0.104	1.07
10	0.009	0.09	1.02

relatively higher percentage of interdendritic areas in this sample due to the higher amount of added copper in it. Comparison of the XRD patterns of as-cast and corresponding dealloyed samples is shown in the Fig. 7(b,c). XRD patterns of the dealloyed samples confirmed absence of the peaks corresponding to the FCC-2 phase thereby confirming removal of copper from interdendritic areas and formation of high entropy foam.

3.3. Electrochemical testing

The effect of insertion of porosity on the electrochemical properties of studied material was evaluated by carrying out cyclic voltammetry (CV) at varying sweep rates (10 – 100 mVs^{-1}). The CV curves of the base HEA and developed foam samples (FS2 and FS3) are shown in Fig. 8. The presence of distinct redox peaks revealed the characteristic pseudocapacitive behavior of the developed material. Insertion of porosity in the CoCrFeNiMn HEA has resulted in a significantly better current response. The effect of scan rate on the cyclic voltammograms was found to be quite significant. The area under the CV curve as well as the current response was found to decrease significantly by decreasing the scan rate from 100 mVs^{-1} to 10 mVs^{-1}. The capacitance values were found to be higher at lower scan rates as diffusion of the electrolyte ions in the electrode was higher which allowed the electrolyte to seep into the whole electrode and store charge at the internal active sites.

The charging/ discharging behavior was analyzed within the potential range − 0.1–0.5 V for FS2 and FS3 electrodes and 0.3–0.5 V for as-cast S1 electrode at 2–10 mA cm^{-2} current densities. The deviation of the charge/discharge curves from the linearity (Fig. 9), mainly due to

Table 3
Comparison of the areal capacitance of various electrode materials from literature with the present study. (CNT: Carbon Nanotubes, NSA: Nanostructured Arrays, VN: Vanadium Nitride, NF: Nickel Foam, ZNPCK: Zinc Gluconate derived activated Porous Carbon, PCG: Pollen derived Carbon/Graphene, CPC: Carbonized Polyimide/Cellulose, NGHPC: Nitrogen doped honeycomb-like Porous Carbon, SSDP: Self-stabilized dispersion polymerization, HrGO: Hydrothermally reduced graphene oxide).

Sr No	Electrode material	Capacitance	Current density / scan rate	Electrolyte	Refs
1	AlCoCrFeNi	0.7 F cm^{-2}	1 mA cm^{-2}	6 M KOH	[45]
2	FeCoNiCuZn	325.17 F g^{-1}	1 A g^{-1}	3 M KOH	[65]
3	PPy/RGO	1.545 F cm^{-2}	0.5 mA cm^{-2}	1 M KCl	[66]
4	SSDP PANI	0.875 F cm^{-2}	1 mA cm^{-2}		[67]
5	HrGO/$SiVW_{11}$	0.377 F cm^{-2}	1.5 mA cm^{-2}		[68]
6	ZnPCK-3	143 F g^{-1}	20 A g^{-1}	6 M KOH	[69]
7	α-Fe_2O_3 nanoparticles	603 F g^{-1}	0.1 A g^{-1}		[70]
8	MnO@CNPs	545 F g^{-1}	0.5 A g^{-1}	6 M KOH	[71]
9	$NiCo_2O_4$ - NCW	1730 F g^{-1}	1 A g^{-1}	1 M KOH	[72]
10	$ZnCl_2$ / Flax based carbon fibers	105 F g^{-1}	1 A g^{-1}		[73]
11	CPC-5	300 F g^{-1}		6 M KOH	[74]
12	**CoCrFeNiMnCu**	**1.563 F cm^{-2}**	**2 mA cm^{-2}**	**2 M KOH**	**This work**

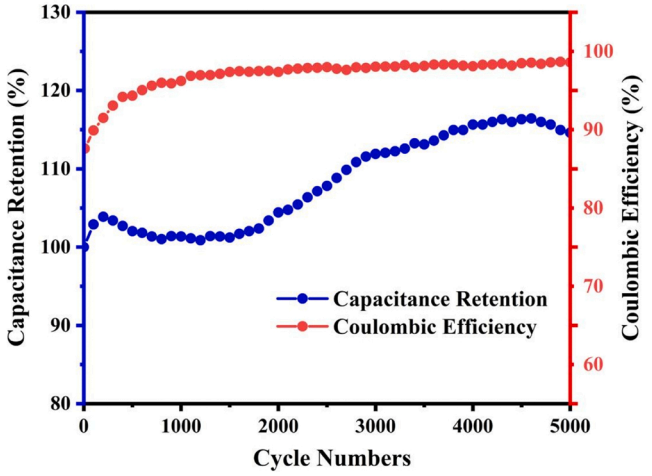

Fig. 10. Cyclic stability of FS2 electrode at 8 mA cm^{-2} current density.

redox reactions, confirmed the pseudocapacitive behavior of electrodes and also corresponded to the redox peaks in CV curves. The longer discharge time of FS3 electrode indicates its higher areal capacitance. The areal capacitances for S1, FS2 and FS3, calculated using Equation 1, was found to be 0.02, 0.260 and 1.56 F cm^{-2} at 2 mA cm^{-2} current density. Values of areal capacitances of S1, FS2, and FS3 at different current densities are given in Table 2. FS3 sample demonstrated areal capacitance of 1.02 F cm^{-2} at a relatively higher current density of 10 mA cm^{-2}, indicating excellent performance and rate capability of the electrode. This high performance could be attributed to the higher amount of porosity and synergistic effects of the elements involved in the HEA electrode [45,63]. The comparison of the areal capacitance of the developed electrode is also shown in Fig. 9(d).

Electrochemical impedance spectroscopy was carried out to further investigate the performance of electrodes. Nyquist plots of electrodes are shown in Fig. 9(e). The inset of the figure shows the equivalent circuit used for fitting the EIS data. EIS was done at 5 mV amplitude and within the frequency range 100 kHz – 10mHz. Nyquist plots for all the electrodes consisted of high-frequency region and low-frequency region. The real axis intercept in the high-frequency region represented the solution resistance (R_s). The diameter of the semicircle in the high-frequency region represented the charge transfer resistance (R_{ct}) at the electrode-electrolyte interface. The R_{ct} values of as-cast S1, FS2, and FS3 electrodes were found to be 416.8 Ω, 24.1 Ω, and 13.17 Ω respectively. The smaller semicircle of FS3 indicated its negligible charge transfer resistance at the electrode-electrolyte interface and high electrical conductivity [64]. This could be attributed to the highly porous structure of the FS3 electrode compared to other electrodes. These results indicated that increasing the amount of porosity linearly decreased the impedance of the electrode. It is believed that the porous structure of the electrode with a short diffusion path provides access to electrolyte ions towards the inside of the electrode which results in lesser resistance. The straight line in the low-frequency region demonstrated the Warburg impedance implying that transportation and adsorption occurred rapidly at the electrode surface. A detailed comparison of areal capacitance values reported in this study with various supercapacitor electrodes from the literature is given in Table 3.

Table 3 illustrates that the areal capacitance of FS3 electrode is significantly higher compared to previously reported values for pseudocapacitive electrodes consisting of similar elements.

The areal capacitance value of the developed FS3 HEA electrode is higher than that of the reported metal/metal oxide, thin films, and HEA-based electrodes. For instance, AlCoCrFeNi nanoporous HEA was fabricated via the selective phase dissolution method and exhibited areal capacitance of 0.7 F cm^{-2} at the current density of 1 mA cm^{-2} [45]. Pristine PANI synthesized through the self-stabilized dispersion polymerization (SSDP) method demonstrated areal capacitance of 0.875 F cm^{-2} at the current density of 1 mA cm^{-2} [67]. PPy/rGO electrodes were fabricated through electrodeposition in a three-electrode system. The developed electrodes exhibited areal capacitance of 1.545 F cm^{-2} at 0.5 mA cm^{-2} current density [66]. The high areal capacitance of the PPy/rGO electrode is attributed to the interconnected structure and high packing density.

Cyclic stability is an important parameter to determine cyclic life and the suitability of electrodes for supercapacitor application. The cyclic stability of the FS3 electrode was evaluated by repeating 5000 charge-discharge cycles at 8 mA cm^{-2} current density as shown in Fig. 10. After 5000 cycles, the electrode retained 114.6% of the initial capacitance indicating excellent cyclic stability of the HEA electrode [45,75]. The coulombic efficiency of 98.6% was exhibited by the electrode.

The outstanding performance of the developed foams can be attributed to the presence of interconnected porosity which allows the electrolyte to access the inner part of the electrode material and have more electroactive sites for the charge storage. Insertion of porosity can improve the charge transfer process by shortening the ion diffusion path. Secondly, theoretical capacitance values of individual components of the selected HEA (Co, Cr, Fe, Ni & Mn) are significantly high. The synergistic effect of these high capacitance components in CoCrFeNiMn foams and the addition of a small amount of copper in the HEA matrix could have enhanced the electrical and ionic conductivity of the electrode. In the present study, the novel electrochemical dealloying process has been adopted for the development of the porous HEAs from as-cast high entropy alloys. Moreover, the electrochemical dealloying process hasn't been previously reported for the development of porous CoCrFeNiMn HEAs. As compared to the reported porous AlCoCrFeNi HEA, the developed porous HEA has demonstrated outstanding electrochemical performance which highlights its high potential as an excellent

candidate for supercapacitors. The developed FS3 porous HEA has exhibited areal capacitance (1.56 F cm^{-2}) which is 2x times higher than the one reported for porous AlCoCrFeNi HEA (0.7 F cm^{-2}) [45] at same current density (2 mA cm^{-2}).

4. Conclusions

CoCrFeNiMn foams have been successfully developed by insertion of copper in the base HEA and its removal by electrochemical dealloying process. Microstructure and crystal structure characterization confirmed the removal of copper from interdendritic areas and the development of interconnected porosity. CoCrFeNiMn foams, developed during the present study, exhibited excellent electrochemical properties. The areal capacitance of the FS3 sample was found to be 1.563 F cm^{-2} at the current density of 2 mA cm^{-2} which is 2x times higher than the one reported for recently developed AlCoCrFeNi HEA foam (0.7 F cm^{-2}) at same current density (2 mA cm^{-2}). FS3 electrode also demonstrated high cyclic stability and exhibited capacitance retention of 114.6% after 5000 cycles at 8 mA cm^{-2} current density. Outstanding electrochemical properties of developed foams were attributed to the presence of interconnected porosity and high entropy effects.

CRediT authorship contribution statement

Talha Abid: Investigations, Formal analysis, Writing – original draft. **M. Aftab Akram**: Formal analysis. **Talha Bin Yaqub**: Writing – review & editing. **M Ramzan Abdul Karim:** Data curation, Writing – review & editing. **Filipe Fernandes:** Data curation, Validation. **Muhammad Farooq Zafar**: Validation. **Khurram Yaqoob:** Conceptualization, Methodology, Software, Supervision, Funding acquisition, Project administration.

Declaration of Competing Interest

The authors declare that they have no known competing financial interests or personal relationships that could have appeared to influence the work reported in this paper.

Data availability

Data will be made available on request.

Acknowledgement

Financial support from Higher Education Commission of Pakistan (HEC NRPU 6019) is acknowledged.

References

[1] W. Deng, Y. Xu, X. Zhang, C. Li, Y. Liu, K. Xiang, H. Chen, NH4) 2Co2V10O28·16H2O/(NH4) 2V10O25·8H2O heterostructure as cathode for high-performance aqueous Zn-ion batteries, J. Alloy. Compd. 903 (2022), 163824, https://doi.org/10.1016/j.jallcom.2022.163824.

[2] W.-N. Deng, Y.-H. Li, D.-F. Xu, W. Zhou, K.-X. Xiang, H. Chen, Three-dimensional hierarchically porous nitrogen-doped carbon from water hyacinth as selenium host for high-performance lithium–selenium batteries, Rare Met. 41 (2022) 3432–3445, https://doi.org/10.1007/s12598-022-02022-0.

[3] D. Li, H. Guo, S. Jiang, G. Zeng, W. Zhou, Z. Li, Microstructures and electrochemical performances of TiO2-coated Mg–Zr co-doped NCM as a cathode material for lithium-ion batteries with high power and long circular life, New J. Chem. 45 (2021) 19446–19455, https://doi.org/10.1039/D1NJ03740D.

[4] W. Zhou, G. Zeng, H. Jin, S. Jiang, M. Huang, C. Zhang, H. Chen, Bio-Template synthesis of V2O3@ carbonized dictyophora composites for advanced aqueous Zinc-Ion batteries, Molecules 28 (2023) 2147, https://doi.org/10.3390/molecules28052147.

[5] Y. Yang, X. Zhang, L. Zhang, W. Zhang, H. Liu, Z. Huang, L. Yang, C. Gu, W. Sun, M. Gao, Recent advances in catalyst-modified Mg-based hydrogen storage materials, J. Mater. Sci. Technol. 163 (2023) 182–211, https://doi.org/10.1016/j.jmst.2023.03.063.

[6] R. Adalati, M. Sharma, S. Sharma, A. Kumar, G. Malik, R. Boukherroub, R. Chandra, Metal nitrides as efficient electrode material for supercapacitors: a review, J. Energy Storage 56 (2022), 105912, https://doi.org/10.1016/j.est.2022.105912.

[7] P. Lamba, P. Singh, P. Singh, P. Singh, A. Kumar, M. Gupta, Y. Kumar, Recent advancements in supercapacitors based on different electrode materials: classifications, synthesis methods and comparative performance, J. Energy Storage 48 (2022), 103871, https://doi.org/10.1016/j.est.2021.103871.

[8] G. Li, X. Lou, C. Peng, C. Liu, W. Chen, Interface chemistry for sodium metal anodes/batteries: a review, Chem. Synth. 2 (2022) 16, https://doi.org/10.20517/cs.2022.19.

[9] C. Ma, X. Wang, J. Lan, J. Zhang, K. Song, J. Chen, J. Ge, W. Chen, Dynamic multistage coupling of FeS2/S enables ultrahigh reversible Na-S batteries, Adv. Funct. Mater. 33 (2023), 2211821, https://doi.org/10.1002/adfm.202211821.

[10] X. He, X. Zhang, A comprehensive review of supercapacitors: properties, electrodes, electrolytes and thermal management systems based on phase change materials, J. Energy Storage 56 (2022), 106023, https://doi.org/10.1016/j.est.2022.106023.

[11] Z. Zhai, L. Zhang, T. Du, B. Ren, Y. Xu, S. Wang, J. Miao, Z. Liu, A review of carbon materials for supercapacitors, Mater. Des. 221 (2022), 111017, https://doi.org/10.1016/j.matdes.2022.111017.

[12] M.R.A. Karim, M. Noman, K.I. Khan, W. Shehzad, E.U. Haq, N. Shahzad, K. Yaqoob, Solvothermal synthesis of flower-flakes like nano composites of Ni-Co metal organic frameworks and graphene nanoplatelets for energy storage applications, ECS J. Solid State Sci. Technol. 11 (2022), 011001, https://doi.org/10.1149/2162-8777/ac44f8.

[13] S.S. Haider, M.Z. Iqbal, S. Zakar, A.M. Afzal, K. Yaqoob, S. Aftab, Superior performance of electrodeposited CoMnS as novel electrode material for supercapattery devices, J. Energy Storage 39 (2021), 102608, https://doi.org/10.1016/j.est.2021.102608.

[14] M.Z. Iqbal, S. Alam, A.M. Afzal, M.J. Iqbal, K. Yaqoob, M.A. Kamran, M.R.A. Karim, T. Alherbi, Binary composites of strontium oxide/polyaniline for high performance supercapattery devices, Solid State Ion. 347 (2020), 115276, https://doi.org/10.1016/j.ssi.2020.115276.

[15] W. Khalid, M.R. Abdul Karim, M. Atif, W. Shehzad, M.A. Marwat, K. Yaqoob, Ultrasounds-assisted solvothermal synthesis of Ni-Co-Mn MOFs/PANI-CNTs nanocomposites with enhanced electrochemical energy storage performance, 0958305×231196126, Energy Environ. (2023), https://doi.org/10.1177/0958305×231196126.

[16] N.N. Loganathan, V. Perumal, B.R. Pandian, R. Atchudan, T.N.J.I. Edison, M. Ovinis, Recent studies on polymeric materials for supercapacitor development, J. Energy Storage 49 (2022), 104149, https://doi.org/10.1016/j.est.2022.104149.

[17] A. Nandagudi, S. Nagarajarao, M. Santosh, B. Basavaraja, S. Malode, R. Mascarenhas, N. Shetti, Hydrothermal synthesis of transition metal oxides, transition metal oxide/carbonaceous material nanocomposites for supercapacitor applications, Mater. Today Sustain. 19 (2022), 100214, https://doi.org/10.1016/j.mtsust.2022.100214.

[18] A. Morenghi, S. Scaravonati, G. Magnani, M. Sidoli, L. Aversa, R. Verucchi, G. Bertoni, M. Riccò, D. Pontiroli, Asymmetric supercapacitors based on nickel decorated graphene and porous graphene electrodes, Electrochim. Acta 424 (2022), 140626, https://doi.org/10.1016/j.electacta.2022.140626.

[19] J. Xiao, H. Li, H. Zhang, S. He, Q. Zhang, K. Liu, S. Jiang, G. Duan, K. Zhang, Nanocellulose and its derived composite electrodes toward supercapacitors: Fabrication, properties, and challenges, J. Bioresour. Bioprod. 7 (2022) 245–269, https://doi.org/10.1016/j.jobab.2022.05.003.

[20] X. Han, G. Xiao, Y. Wang, X. Chen, G. Duan, Y. Wu, X. Gong, H. Wang, Design and fabrication of conductive polymer hydrogels and their applications in flexible supercapacitors, J. Mater. Chem. A 8 (2020) 23059–23095, https://doi.org/10.1039/D0TA07468C.

[21] L. Yang, X. Guo, Z. Jin, W. Guo, G. Duan, X. Liu, Y. Li, Emergence of melanin-inspired supercapacitors, Nano Today 37 (2021), 101075, https://doi.org/10.1016/j.nantod.2020.101075.

[22] Y. Wang, L. Zhang, H. Hou, W. Xu, G. Duan, S. He, K. Liu, S. Jiang, Recent progress in carbon-based materials for supercapacitor electrodes: a review, J. Mater. Sci. 56 (2021) 173–200, https://doi.org/10.1007/s10853-020-05157-6.

[23] F. Wang, J. Lee, L. Chen, G. Zhang, S. He, J. Han, J. Ahn, J.Y. Cheong, S. Jiang, I.-D. Kim, Inspired by wood: Thick electrodes for supercapacitors, ACS Nano 17 (2023) 8866–8898, https://doi.org/10.1021/acsnano.3c01241.

[24] I.U. Hassan, H. Salim, G.A. Naikoo, T. Awan, R.A. Dar, F. Arshad, M.A. Tabidi, R. Das, W. Ahmed, A.M. Asiri, A review on recent advances in hierarchically porous metal and metal oxide nanostructures as electrode materials for supercapacitors and non-enzymatic glucose sensors, J. Saudi Chem. Soc. 25 (2021), 101228, https://doi.org/10.1016/j.jscs.2021.101228.

[25] Z.U. Rehman, M.A. Raza, A. Tariq, U.N. Chishti, M.F. Maqsood, N. Lee, M.H. Awais, S.M.Z. Mehdi, A. Inam, La0.75Sr0.25Cr0.5Mn0.5O3 perovskite developed for supercapacitor applications, J. Energy Storage 32 (2020), 101951, https://doi.org/10.1016/j.est.2020.101951.

[26] B. Li, K. Zhang, S. Qi, Y. Guo, J. Chen, Y. Lou, Hierarchical ZnCo2O4-ZnO/ZnCo2O4 core-shell microarchitecture as pseudocapacitive material with ultra-high rate capability and enhanced cyclic stability for asymmetric supercapacitors, Appl. Surf. Sci. 592 (2022), 153202, https://doi.org/10.1016/j.apsusc.2022.153202.

[27] K. Yang, Q. Fan, C. Song, Y. Zhang, Y. Sun, W. Jiang, P. Fu, Enhanced functional properties of porous carbon materials as high-performance electrode materials for supercapacitors, Green. Energy Resour. 1 (2023), 100030, https://doi.org/10.1016/j.gerr.2023.100030.

[28] K. Sudhakar, P. Rajeswaran, T. Kamatchi, S. Ambika, Facile one-pot synthesis of porous NiCoP@ reduced graphene oxide composite as active electrode material for

high energy density asymmetric supercapacitor, Chem. Phys. Lett. 826 (2023), 140635, https://doi.org/10.1016/j.cplett.2023.140635.
[29] E. Bao, X. Ren, R. Wu, X. Liu, H. Chen, Y. Li, C. Xu, Porous MgCo2O4 nanoflakes serve as electrode materials for hybrid supercapacitors with excellent performance, J. Colloid Interface Sci. 625 (2022) 925–935, https://doi.org/10.1016/j.jcis.2022.06.098.
[30] J. Yang, C. Wang, D. Xie, H. Qin, W. Liu, M. Liang, X. Li, C. Liu, M. Huang, A new type of gradient structure FeCoCrNiWMo high entropy alloy layer by plasma solid-state surface metallurgy, Surf. Coat. Technol. 457 (2023), 129320, https://doi.org/10.1016/j.surfcoat.2023.129320.
[31] X. Zhou, J. Chen, R. Ding, H. Wu, S. Lu, J. He, W. Wang, H. Pan, A novel coherent particles-reinforced FCC-based high-entropy superalloy with superior high-temperature compressive properties, Mater. Sci. Eng. A 872 (2023), 144947, https://doi.org/10.1016/j.msea.2023.144947.
[32] X. Zhou, J. Chen, R. Ding, H. Wu, S. Lu, J. He, H. Pan, Effect of Mn on microstructure and tensile properties of as-cast Al0.5CoFeNiC0.1 high-entropy alloy, Mater. Sci. Eng. A 873 (2023), 144951, https://doi.org/10.1016/j.msea.2023.144951.
[33] J. Zhu, M. Lv, C. Liu, X. Tan, H. Xu, Effect of neodymium and yttrium addition on microstructure and DC soft magnetic property of dual-phase FeCoNi(CuAl)0.8 high-entropy alloy, J. Rare Earths 41 (2022) 1562–1567, https://doi.org/10.1016/j.jre.2022.06.005.
[34] K. Li, Y. Zhai, M. Lai, M. Song, S. Zou, G. Huang, K. Yaqoob, Z. Wang, N. Zhang, Corrosion of eutectic high-entropy alloys: a review, Crystals 13 (2023) 1231, https://doi.org/10.3390/cryst13081231.
[35] M. Abdullah, M. Mukarram, T.B. Yaqub, F. Fernandes, K. Yaqoob, Development of eutectic high entropy alloy by addition of W to CoCrFeNi HEA, Int. J. Refract. Met. Hard Mater. 115 (2023), 106300, https://doi.org/10.1016/j.ijrmhm.2023.106300.
[36] M.A. Mehmood, M. Mujahid, A. Godfrey, M.F. Zafar, K. Yaqoob, Development and characterization of boride-reinforced CoCrFeNi composites, J. Alloy. Compd. 947 (2023), 169535, https://doi.org/10.1016/j.jallcom.2023.169535.
[37] M.A. Mehmood, K. Shehzad, M. Mujahid, T.B. Yaqub, A. Godfrey, F. Fernandes, F. Muhammad, K. Yaqoob, Ceramic-reinforced HEA matrix composites exhibiting an excellent combination of mechanical properties, Sci. Rep. 12 (2022), 21486, https://doi.org/10.1038/s41598-022-25734-w.
[38] S.W. Hussain, M.A. Mehmood, M.R.A. Karim, A. Godfrey, K. Yaqoob, Microstructural evolution and mechanical characterization of a WC-reinforced CoCrFeNi HEA matrix composite, Sci. Rep. 12 (2022), 9822, https://doi.org/10.1038/s41598-022-13649-5.
[39] M. Mukarram, M.A. Munir, M. Mujahid, K. Yaqoob, Systematic development of eutectic high entropy alloys by thermodynamic modeling and experimentation: an example of the CoCrFeNi-Mo system, Metals 11 (2021) 1484, https://doi.org/10.3390/met11091484.
[40] M. Mukarram, M. Mujahid, K. Yaqoob, Design and development of CoCrFeNiTa eutectic high entropy alloys, J. Mater. Res. Technol. 10 (2021) 1243–1249, https://doi.org/10.1016/j.jmrt.2020.12.042.
[41] D. Liu, J. Hou, X. Jin, X. Wang, H. Yang, J. Qiao, The cobalt-free Fe35Mn15Cr15Ni25Al10 high-entropy alloy with multiscale particles for excellent strength-ductility synergy, Intermetallics 163 (2023), 108064, https://doi.org/10.1016/j.intermet.2023.108064.
[42] E.E. Nettey-Oppong, E.E. Mensah, E. Effah, E. Asare, M.A. Nartey, Mechanical properties and deformation behavior of equiatomic CoCrFeMnNi high-entropy alloy foam: A molecular dynamics study, Solid State Commun. 371 (2023), 115236, https://doi.org/10.1016/j.ssc.2023.115236.
[43] L. Fang, J. Wang, X. Li, X. Tao, Y. Ouyang, Y. Du, Effect of Cr content on microstructure characteristics and mechanical properties of ZrNbTaHf0.2Crx refractory high entropy alloy, J. Alloy. Compd. 924 (2022), 166593, https://doi.org/10.1016/j.jallcom.2022.166593.
[44] J. Shi, Y. Zhang, X. Wang, C. Jiang, M. Wang, C. Ma, H. Huang, Microstructure and mechanical properties of UNbTiHf1-xMox high-entropy alloys, Mater. Sci. Eng. A 860 (2022), 144239, https://doi.org/10.1016/j.msea.2022.144239.
[45] K. Kong, J. Hyun, Y. Kim, W. Kim, D. Kim, Nanoporous structure synthesized by selective phase dissolution of AlCoCrFeNi high entropy alloy and its electrochemical properties as supercapacitor electrode, J. Power Sources 437 (2019), 226927, https://doi.org/10.1016/j.jpowsour.2019.226927.
[46] F. Wang, D. Zhao, B. Li, W. Li, H. Zhang, J. Pang, L. Fan, Compositional engineering of Co(II) MOF/carbon-based overall water splitting electrocatalysts: From synergistic effects to structure–activity relationships, Cryst. Growth Des. 22 (2022) 2775–2792, https://doi.org/10.1021/acs.cgd.2c00168.
[47] L.B. Serrano, M. Moussa, J.-Y. Yao, G. Silva, J.-L. Bobet, S.S. Ferreira, K.R. Cardoso, Development of Ti-V-Nb-Cr-Mn high entropy alloys for hydrogen storage, J. Alloy. Compd. 945 (2023), 169289, https://doi.org/10.1016/j.jallcom.2023.169289.
[48] N. Sreenivasulu, U.N. Kumar, K.M. Madhav, T. Thomas, S. Bhattacharya, Structural and electrochemical investigations on nanocrystalline high entropy spinel oxides for battery-like supercapacitor applications, ChemistrySelect 7 (2022), e202104015, https://doi.org/10.1002/slct.202104015.
[49] B. Bounor, J.S. Seenath, S.G. Patnaik, D. Bourrier, C.C.H. Tran, J. Esvan, L. Weingarten, A. Descamps-Mandine, D. Rochefort, D. Guay, Low-cost micro-supercapacitors using porous Ni/MnO2 entangled pillars and Na-based ionic liquids, Energy Storage Mater. 63 (2023), 102986, https://doi.org/10.1016/j.ensm.2023.102986.
[50] F.-z Tan, M.-t Ma, W.-j Cai, Y.-l Chen, Y.-h Wang, J.-h Zhou, Synthesis of porous biocarbon supported Ni3S4/CeO2 nanocomposite as high-efficient electrode materials for asymmetric supercapacitors, J. Saudi Chem. Soc. 26 (2022), 101530, https://doi.org/10.1016/j.jscs.2022.101530.
[51] Y. Gao, Y. Xia, H. Wan, X. Xu, S. Jiang, Enhanced cycle performance of hierarchical porous sphere MnCo2O4 for asymmetric supercapacitors, Electrochim. Acta 301 (2019) 294–303, https://doi.org/10.1016/j.electacta.2019.01.173.
[52] X.-L. Zhang, W.-B. Zhang, Y. Yin, M.M. Theint, S.-B. Guo, S.-S. Chai, X. Zhou, X.-J. Ma, Sol-gel method preparation and high-rate energy storage of high-entropy ceramic (FeCoCrMnNi)C porous powder, Ceram. Int. 49 (2023) 29327–29338, https://doi.org/10.1016/j.ceramint.2023.06.228.
[53] P. Forouzandeh, P. Ganguly, R. Dahiya, S.C. Pillai, Supercapacitor electrode fabrication through chemical and physical routes, J. Power Sources 519 (2022), 230744, https://doi.org/10.1016/j.jpowsour.2021.230744.
[54] M. Fu, X. Ma, K. Zhao, X. Li, D. Su, High-entropy materials for energy-related applications, Iscience 24 (2021), 102177, https://doi.org/10.1016/j.isci.2021.102177.
[55] Y. Wang, Y. Wang, High-entropy alloys in catalyze and supercapacitors: a review, Nano Energy 104 (2022), 107958, https://doi.org/10.1016/j.nanoen.2022.107958.
[56] Y. Yuan, Z. Xu, P. Han, Z. Dan, F. Qin, H. Chang, MnO2-decorated metallic framework supercapacitors fabricated from duplex-phase FeCrCoMnNiAl0.75 Cantor high entropy alloy precursors through selective phase dissolution, J. Alloy. Compd. 870 (2021), 159523, https://doi.org/10.1016/j.jallcom.2021.159523.
[57] P. Tang, Y. Cao, M. Lu, W. Qiu, The preparation of high-performance aqueous supercapacitor with high-entropy pyrochlore-type electrode and super-concentrated electrolyte, Ceram. Int. 48 (2022) 2660–2669, https://doi.org/10.1016/j.ceramint.2021.10.050.
[58] Y. Wu, K. Luo, Y. Zhang, C. Kong, H. Yu, Microstructures and mechanical properties of a CoCrFeNiMn high-entropy alloy obtained by 223 K cryorolling and subsequent annealing, J. Alloy. Compd. 921 (2022), 166166, https://doi.org/10.1016/j.jallcom.2022.166166.
[59] C. Liu, X. Jiang, H. Sun, Y. Zhang, Y. Fang, R. Shu, Microstructure and mechanical properties of bioinspired laminated CoCrFeNiMn high entropy alloy matrix composites reinforced with graphene, Mater. Sci. Eng. A 859 (2022), 144198, https://doi.org/10.1016/j.msea.2022.144198.
[60] P. Wang, P. Huang, F.L. Ng, W.J. Sin, S. Lu, M.L.S. Nai, Z. Dong, J. Wei, Additively manufactured CoCrFeNiMn high-entropy alloy via pre-alloyed powder, Mater. Des. 168 (2019), 107576, https://doi.org/10.1016/j.matdes.2018.107576.
[61] E.S. Park, K. Yoon, K. Yaqoob, J.I. Lee, J.Y. Kim, High-entropy alloy foam and manufacturing method for the foam, in: U. Patent (Ed.) 2021.
[62] T. Nagase, A. Shibata, M. Matsumuro, M. Takemura, S. Semboshi, Alloy design and fabrication of ingots in Cu-Zn-Mn-Ni-Sn high-entropy and Cu-Zn-Mn-Ni medium-entropy brasses, Mater. Des. 181 (2019), 107900, https://doi.org/10.1016/j.matdes.2019.107900.
[63] M. Lan, X. Wang, R. Zhao, M. Dong, L. Fang, L. Wang, Metal-organic framework-derived porous MnNi2O4 microflower as an advanced electrode material for high-performance supercapacitors, J. Alloy. Compd. 821 (2020), 153546, https://doi.org/10.1016/j.jallcom.2019.153546.
[64] A.T. Prasannakumar, R. Rohith, J. Cherusseri, R.R. Mohan, S. Varma, High areal capacitance and long cycling stability in asymmetric supercapacitors using binder-free, hierarchical nanostructured Ni3S2/MnO2 hybrid electrodes, J. Energy Storage 55 (2022), 105723, https://doi.org/10.1016/j.est.2022.105723.
[65] G.C. Mohanty, C.C. Gowda, P. Gakhad, M. Sanjay, S. Chowdhury, K. Biswas, A. Singh, C.S. Tiwary, Iron-Cobalt-Nickel-Copper-Zinc (FeCoNiCuZn) high entropy alloy as positive electrode for high specific capacitance supercapacitor, Electrochim. Acta (2023), 143272, https://doi.org/10.1016/j.electacta.2023.143272.
[66] F. Dang, W. Zhao, W. Tong, P. Yang, D. Wang, Y. Liu, Extrinsic design of high-performance programmable supercapacitor with large specific areal capacitance, Electrochim. Acta 463 (2023), 142845, https://doi.org/10.1016/j.electacta.2023.142845.
[67] T.P. Anandhu, R.R. Mohan, J. Cherusseri, R. Rohith, S.J. Varma, High areal capacitance and enhanced cycling stability of binder-free, pristine polyaniline supercapacitor using hydroquinone as a redox additive, Electrochim. Acta 425 (2022), 140740, https://doi.org/10.1016/j.electacta.2022.140740.
[68] B.R. Biradar, S. Maity, P.R. Chandewar, D. Shee, P.P. Das, S.S. Mal, High areal capacitance polyoxotungstate-reduced graphene oxide-based supercapacitors, Inorg. Chem. Commun. 155 (2023), 110987, https://doi.org/10.1016/j.inoche.2023.110987.
[69] G. Duan, J. Xiao, L. Chen, C. Zhang, S. Jian, S. He, F. Wang, Zinc gluconate derived porous carbon electrode assisted high rate and long cycle performance supercapacitor, J. Energy Storage 67 (2023), 107559, https://doi.org/10.1016/j.est.2023.107559.
[70] G. Duan, H. Zhang, C. Zhang, S. Jiang, H. Hou, High mass-loading α-Fe2O3 nanoparticles anchored on nitrogen-doped wood carbon for high-energy-density supercapacitor, Chin. Chem. Lett. 34 (2023), 108283, https://doi.org/10.1016/j.cclet.2023.108283.
[71] W. Guo, X. Guo, L. Yang, T. Wang, M. Zhang, G. Duan, X. Liu, Y. Li, Synthetic melanin facilitates MnO supercapacitors with high specific capacitance and wide operation potential window, Polymers 235 (2021), 124276, https://doi.org/10.1016/j.polymer.2021.124276.
[72] J. Yang, H. Li, S. He, H. Du, K. Liu, C. Zhang, S. Jiang, Facile electrodeposition of NiCo2O4 nanosheets on porous carbonized wood for wood-derived asymmetric supercapacitors, Polymers 14 (2022) 2521, https://doi.org/10.3390/polym14132521.

[73] G. Duan, L. Zhao, L. Chen, F. Wang, S. He, S. Jiang, Q. Zhang, ZnCl2 regulated flax-based porous carbon fibers for supercapacitors with good cycling stability, New J. Chem. 45 (2021) 22602–22609, https://doi.org/10.1039/D1NJ04667E.
[74] H. Li, L. Cao, H. Zhang, Z. Tian, Q. Zhang, F. Yang, H. Yang, S. He, S. Jiang, Intertwined carbon networks derived from Polyimide/Cellulose composite as porous electrode for symmetrical supercapacitor, J. Colloid Interface Sci. 609 (2022) 179–187, https://doi.org/10.1016/j.jcis.2021.11.188.
[75] Y. Ouyang, B. Zhang, C. Wang, X. Xia, W. Lei, Q. Hao, Bimetallic metal-organic framework derived porous NiCo2S4 nanosheets arrays as binder-free electrode for hybrid supercapacitor, Appl. Surf. Sci. 542 (2021), 148621, https://doi.org/10.1016/j.apsusc.2020.148621.